Intracrater sediment trapping and transport in Arabia Terra, Mars

Taylor Christopher Dorn[1] and Mackenzie Day[1]

[1]University of California Los Angeles

November 26, 2022

Abstract

Craters are the most prevalent basins and potential depo-centers of sediment on Mars. Within these craters and extending from them, terminal dune fields and wind streaks are abundant, indicating active sediment transport and providing a way to study how wind and sediment interact with crater topography. Here, we explore the role of craters as both sources and sinks in the modern martian sedimentary cycle. Our results show that craters with low albedo wind streaks (indicative of active transport out of a crater) have lower crater wall slopes ($9.4° \pm 5.5°$) compared to craters without wind streaks ($17° \pm 5.8°$). We interpret that crater wall slopes play a dominant role in sediment transport out of a crater basin, and infer, from measurements of craters on Mars, that a crater transitions from being a net sediment sink to a net sediment source when crater wall slopes reach ˜15°. This threshold value is consistent with limits of bedform climb observed on Earth and elsewhere on Mars.

1   **Intracrater sediment trapping and transport in Arabia Terra, Mars**

2   **Taylor Dorn and Mackenzie Day**

3   Department of Earth, Planetary, and Space Sciences, University of California Los Angeles

4   Corresponding author: Taylor Dorn (planetarytaylor@g.ucla.edu)
5

6   **Key Points:**

7   - The slope of a crater wall plays a dominant role in sediment trapping by a crater

8   - Craters associated with low albedo wind streaks have lower crater wall slopes compared
9   to craters without wind streaks

10 - A crater transitions from being a sink to a source of sediment when the crater wall slope
11   is between 10° and 20°, most commonly at ~15°

12

13   **Abstract**

14   Craters are the most prevalent basins and potential depo-centers of sediment on Mars. Within
15   these craters and extending from them, terminal dune fields and wind streaks are abundant,
16   indicating active sediment transport and providing a way to study how wind and sediment
17   interact with crater topography. Here, we explore the role of craters as both sources and sinks in
18   the modern martian sedimentary cycle. Our results show that craters with low albedo wind
19   streaks (indicative of active transport out of a crater) have lower crater wall slopes (9.4° ±5.5°)
20   compared to craters without wind streaks (17° ±5.8°). We interpret that crater wall slopes play a
21   dominant role in sediment transport out of a crater basin, and infer, from measurements of craters
22   on Mars, that a crater transitions from being a net sediment sink to a net sediment source when
23   crater wall slopes reach ~15°. This threshold value is consistent with limits of bedform climb
24   observed on Earth and elsewhere on Mars.
25

26   **Plain Language Summary**

27   Craters can collect sediment and are prevalent on Mars. Dune fields, within craters, and wind
28   streaks, outside of craters, show that sediment is actively being transported and provide a way to
29   study how wind and sediment interact with craters. Here, we focus on craters that have interior
30   dune fields to understand sediment being transported out of a crater. Our measurements of crater
31   wall slopes show that the slope of the wall primarily determines whether sediment can escape
32   from a crater. We conclude that craters transition from trapping sediment to losing sediment
33   when crater wall slopes reach ~15°.

34   **1 Introduction**

35   The transport of sediments on the modern martian surface is dominantly driven by
36   aeolian processes. Modern sand-transporting winds form fields of aeolian bedforms and erode
37   exposed bedrock into yardangs, ventifacts, or periodic bedrock ridges (Ward, 1979; Montgomery
38   et al., 2012; Bridges, 2014). Discoveries of ancient aeolian sandstones on Mars (Grotzinger et al.,
39   2005; Banham et al., 2018; Day et al., 2019) show that aeolian transport on Mars has been
40   prevalent throughout the planet's history. Modern erosion of these and other sedimentary
41   formations by wind has remobilized ancient sediments, adding to the global sediment budget and
42   forming a martian sedimentary rock cycle (Malin and Edgett, 2000; Grotzinger and Milliken,
43   2012; McLennan et al., 2019). However, the conditions on Mars have changed significantly over
44   the past several billion years (see review in Wordsworth, 2016), and mechanisms of sedimentary
45   rock accumulation preservation that were available in the Noachian (e.g., trapping or
46   cementation by water) are no longer available today.

47   Geomorphic evidence of surface-wind interactions is abundant on Mars and includes
48   aeolian bedforms (Balme et al., 2008; Ewing and Kocurek, 2010; Hayward et al., 2014),
49   yardangs (Ward, 1979; Zimbelman and Griffin, 2010; Urso et al., 2018), wind streaks (Veverka
50   et al., 1981; Lee, 1984; Edgett, 2002), and dust devil tracks (Greeley et al., 2006). In particular,
51   dunes and wind streaks commonly interact with crater topography and provide a mechanism to
52   study how wind and sediment transport interact with these local depo-centers. Wind streaks,
53   linear features that align in the direction of wind transport, taper downwind from a topographic
54   obstacle or sediment source (Thomas et al., 1981; Lee, 1984). Wind streaks are primarily
55   classified by their albedo contrast with the surrounding terrain, where high albedo wind streaks

56 reflect dust deposition on the surface and low albedo wind streaks reflect the removal of surface
57 dust (Thomas et al., 1981; Veverka et al., 1981).

58   Dunes form when sufficient volumes of sand accumulate in an active wind regime. These
59 bedforms exhibit a crestline, which, along with the bedform morphology, reflect the direction
60 and complexity of the local wind (McKee, 1979; Rubin and Hunter, 1987; Ewing and Kocurek,
61 2010; Courrech du Pont, et al., 2014). Actively migrating dunes have been identified on Mars
62 (Fenton, 2006; Silvestro et al., 2010; Chojnacki et al., 2017) and commonly form large fields
63 covering many tens of square kilometers. These active bedforms are typically dust-free and
64 basaltic in composition (Edgett and Lancaster, 1993; Achilles et al., 2017), causing them to
65 appear very dark in imaging with respect to their dusty surroundings.

66   Dune fields require significant volumes of sand to develop, and local topography can aid
67 in sand accumulation. Steep topography (e.g., a mountain or crater wall) impedes sediment
68 transport and dune migration, creating a depo-center for sand that may develop into a trapped or
69 "terminal" dune field (Hesse, 2009). On Earth, examples of terminal dune fields include the
70 Great Sand Dunes, CO (Fryberger et al, 1979) and Kelso Dunes, CA (Sharp, 1966), each
71 topographically bound by local mountain ranges. On Mars, craters provide both local basins in
72 which sediment can be deposited, and topographic obstacles (i.e., the walls of the crater) behind
73 which dune fields can become trapped.

74   In order to understand martian sediment cycling in modern conditions, we must
75 understand where accumulation takes place. Are aeolian sands continually transported around the
76 planet, or are there local depo-centers that serve as permanent traps for wind-blown material?
77 The most prevalent basins and potential depo-centers on Mars are craters. In this work, we
78 explore the role of craters as both sources and sinks of aeolian sediment in the modern martian
79 sedimentary cycle using evidence of aeolian transport from wind streaks and intra-crater dune
80 fields. Although polar processes also play an important role in the modern and ancient sediment
81 budget, this work focuses on the equatorial and mid-latitude region of Arabia Terra and,
82 therefore, does not consider the role of ice. Intra-crater dune fields and intercrater plain wind
83 streaks are abundant in Arabia Terra, making the region ideal for studying aeolian-crater
84 dynamics. Our findings indicate that the slope of a crater's wall plays a significant role in
85 determining whether a crater is a sink or a source of sediment.

86 **2 Methods**

87   To understand the dynamics of sand transport into and out of craters, we identified 116
88 craters with diameters >10 km in Arabia Terra where terminal dune fields were observed within
89 the crater's interior (Fig. 1; Robbins and Hynek, 2012). Dune fields were considered terminal if
90 the nearest crater wall to the dune field was located in the downwind direction. All dune fields
91 were large enough to include multiple bedforms. Wind directions were interpreted from the dune
92 morphology and crestline orientation (McKee, 1979; Rubin and Hunter, 1987; Kocurek and
93 Ewing, 2005). Crater diameters, dune fields, and interpreted wind directions were mapped using
94 ArcMap 10.6 on a mosaic of images from the Mars Reconnaissance Orbiter (MRO) Context
95 Camera (CTX) (Malin et al., 2007) with a resolution of ~6 m/px provided by the Murray Lab
96 (Dickson et al., 2018).

97   Craters were categorized based on the presence or absence of evidence suggesting that
98 sediment was being transported out of the crater. In many cases, craters with interior dune fields
99 were associated with wind streaks (Fig. 2a), indicating that there is recent sediment transport out

100   of the crater. In other cases, no wind streak or other crater-scale evidence of extra-crater
101   transport was observed (Fig. 2b). Prevailing wind directions were interpreted and mapped using
102   dune morphologies, their position within the craters, and wind streak orientation (Fig. 1).

103   Crater wall slopes were measured downwind of each terminal dune field using elevation
104   data from the Mars Orbiter Laser Altimeter (MOLA) 128 ppd interpolated elevation map (Smith
105   et al., 2001). The slope of each crater wall was measured at the closest location downwind of
106   each terminal dune field from a wind-parallel elevation transect originating at the rim of the
107   crater down to the dune field. The maximum slope was most often near the crater rim as the
108   slope decreased along the transect to the dunes on the crater floor. Because this work focuses on
109   how crater wall slopes affect sediment transport, the maximum measured slope is discussed and
110   the reported crater wall slopes are the most steeply dipping slope that sediment from a given
111   crater encounters during transport up each crater wall.

112   3 Results

113   We identified 116 craters in Arabia Terra with interior terminal dune fields. From this
114   dataset, 55 craters have wind streaks emanating from their crater rim onto the surrounding terrain
115   while 61 craters have no wind streaks present. Among the 55 craters that are associated with a
116   wind streak, 39 craters have low albedo wind streaks emanating from the rim while the
117   remaining 16 craters have high albedo wind streaks extending into the surrounding plains. The
118   crater wall slope was measured in each of the 116 craters studied (Table 1), downwind of each
119   terminal dune field. Craters displaying a low albedo wind streak have a lower average slope (9.4°
120   ± 5.5°; n=39) compared to craters without an associated wind streak (17.0° ± 5.8°, n=61) (Fig. 3;
121   Table 1). Craters displaying high albedo wind streaks have higher average slopes compared to
122   the previous two crater populations (24.4° ± 9.6°, n=16).

123   Crater diameters were also measured in each of the 116 craters selected for this study
124   (Table 2) and showed that the presence or absence of wind streaks was not associated with a
125   particular crater diameter. The dune fields are dominantly in the south to southwest region within
126   each crater; with dune slipfaces predominantly oriented towards the southwest. Individual wind
127   streaks maintain the same relative albedo contrast and orientation across multiple CTX images
128   covering the streaks at different times. The orientation of the wind streaks in the area was
129   consistently towards the south (Fig. 4), consistent with wind directions interpreted from the dune
130   fields and indicating largely southward sediment transport across Arabia Terra. Some evidence
131   of active transport was observed in small bedforms or sand sheets that changed between time-
132   separated images in both CTX and High Resolution Imaging Science Experiment (HiRISE;
133   McEwen et al., 2007) images (e.g., Fig 5).

134   4 Discussion

135   Craters studied within this work demonstrate a range of interactions between aeolian
136   sediment transport and crater basin topography. Each crater, by requirement, is occupied by a
137   low albedo dune field interpreted as evidence of active sediment transport within the crater basin
138   (Edgett, 2002; Silvestro et al., 2010; Chojnacki et al., 2011, 2015; Bridges et al., 2017). Around
139   half of the studied craters are associated with either a low or high albedo wind streak, indicating
140   that, in these instances, sediment is transported out of the crater. The remaining craters, not
141   associated with a wind streak, represent basins with active transport in their interior, but no
142   sediment transfer to the surrounding plains. These two end members, craters where sediment is

143   transported out of the crater and craters that trap sediment, represent basins acting as sources and
144   sinks of sediment, respectively. The results of this study indicate that transport out of the basin is
145   primarily influenced by the slope of the crater walls.

4.1 Craters transitioning from a sink to a source of sediment

147   The results of this work show that craters with different sediment trapping properties
148   exhibit statistically distinct crater wall slopes. Focusing only on the downwind crater wall where
149   wind-blown sand would encounter topography, craters with low albedo wind streaks, indicative
150   of active saltation outside of the crater rim, have wall slopes averaging $9.4° \pm 5.5°$, ranging
151   between ~ $0°$ and ~$18°$ (Fig. 3; Table 1). Craters with low albedo wind streaks also exhibited an
152   average diameter of 49 ± 23 km and a d/D of 0.03 ± 0.01 (Table 2). Craters without wind streaks,
153   considered to be sinks, have much steeper crater wall slopes and are smaller in diameter, when
154   compared to craters with low albedo wind streaks, averaging a slope of $17.0° \pm 5.8°$ and an
155   average diameter of 32 ± 22 km (Fig. 3; Table 1). A two-sample t-test conducted for the crater
156   wall slopes, crater diameters, and d/D found that these two crater populations were statistically
157   distinct with >95% confidence. Intuitively, these results demonstrate that younger craters with
158   steeper wall slopes serve as sediment traps, prohibiting aeolian material from escaping, whereas
159   older craters with shallower slopes are better suited for sediment transport out of the basin,
160   serving as an input or source to the surrounding plains and the global sediment budget.

161   Observations of craters in this work suggest that the transition from sink to source that
162   occurs when crater wall slopes reach between $10° - 18°$ (Fig. 3). At ~$10°$ we simultaneously see
163   a decrease in the number of craters with low albedo wind streaks and an increase in the number
164   of craters without wind streaks. There are no craters with low albedo wind streaks that have
165   crater wall slopes above $18°$, and we speculate that the transition from terminal sink to a
166   sediment source occurs when crater wall slopes approach this value.

167   To better understand when sediment transport out of a crater becomes possible, we
168   looked at the downwind-most bedforms in craters with wall slopes in this transitional range of
169   $10° - 18°$. In eight of the 45 craters in this transitional range, dunes were found migrating up
170   crater walls (Fig. 6). These eight craters have an average wall slope of ~$14°$ and do not have low
171   albedo wind streaks emanating from the crater rim. We interpret this crater population to
172   represent the transition from a crater sink to a source; a stage when significant transport is
173   occurring on the crater wall, but sediment is still largely unable to escape the crater. Dunes
174   shown in Figure 6c are migrating on a crater wall slope measured locally at ~$5.7°$ (the steepest
175   slope measured on this crater wall is ~$16°$, ~2 km downslope of the crater rim. The morphology
176   of these and nearby dunes suggests local scale reversal in transport direction, such that the dunes
177   are sometimes migrating up the wall and sometimes falling back down. Climbing dunes have
178   also been identified elsewhere on Mars. In Valles Marineris, dunes were found migrating up the
179   north wall of Melas Chasma on slopes of up to $15°$, similar to the limit suggested here in the
180   observed transitional craters (Chojnacki et al., 2010).

181   Dust and fine sediment are abundant on Mars (Malin and Edgett, 2000), and dust
182   transport out of craters may occur even when sand removal does not. For example, the 16 craters
183   in this work associated with high albedo wind streaks could be examples of basins from which
184   dust is removed but sand sized grains are not. The mean slope measured in this population,
185   $24.4°$, falls well above the mean of craters with dark wind streaks ($9.4°$), suggesting that high
186   wall slopes are not an impediment to all sediment removal. We speculate that the distinction
187   between these bright wind streaks and the craters with no streaks at all reflects the local

188 availability of dust in the crater, or the dynamics of turbulent eddies formed as wind interacts
189 with crater topography.

190   Within the low albedo wind streaks, evidence of recent sediment transport can be
191 observed at meter- and deca-meter scales (Fig. 7). In cases where a wind streak is interrupted by
192 another kilometer-scale basin, dark dunes were found within low albedo wind streak (Fig. 7a).
193 Elsewhere, dark sand sheets accumulate in rugged topography and smaller dunes are found in
194 craters in the wind streaks (Figs. 5, 7b). Changes in these sand sheets between successive CTX
195 images demonstrate that aeolian sediment transport is actively occurring in these plains.

196 ### *4.2 Crater degradation on Mars*

197   Fresh craters have sharply defined rims and steep slopes that degrade over time. Crater
198 wall slopes have been measured on the Moon (Stopar et al., 2017), Mars (Craddock et al., 1997),
199 and Earth (Grant and Schultz, 1993), and occur with initial wall slopes at or above the angle of
200 repose (~30°). The material forming crater rims includes competent rock, enabling crater walls to
201 hold initially steep slopes that can even locally be vertical (e.g., Grant and Schultz, 1993). The
202 majority of slope-reducing crater degradation on Mars occurred in the Noachian when fluvial
203 processes drove topographic diffusion (Grant and Schultz, 1993; Kreslavsky and Head, 2006).
204 Since the Noachian, degradation of craters of the size studied in this work (>10 km in diameter)
205 has been relatively minimal (Robbins et al., 2013). Recent work studying crater wall slopes on
206 Mars found that craters in Hesperian and Amazonian terrains dominantly exhibited wall slopes
207 of >20° with the steepest at ~30° (Kreslavsky and Head, 2018). Crater wall slopes of ~15°,
208 representing the transition from sink to source based on this work, were characteristic of late
209 Noachian crater formation and associated degradation (Mangold et al., 2012). This suggests that
210 craters formed since the Noachian-Hesperian transition, a time of significant climatic shift on
211 Mars (Wordsworth, 2016), are net sinks of sediment that trap aeolian material and reduce the
212 overall mobile sediment budget.

213   Changes in atmospheric density and variability in the wind regime would also have
214 influenced the trapping role of sedimentary basins over time. The presence of water, in addition
215 to causing significant crater degradation, would have made craters more effective sediment traps
216 if lakes or wet surfaces were present in their interior (Newsom et al., 1996; Cabrol and Grin,
217 1999; Catling, 1999; McLennan et al., 2005). Changes in wind regime would alter the path of
218 aeolian sediments across a crater, but the direction of sand transporting winds appears to have
219 changed very little in the course of human observation. In the past decade of observation with
220 CTX, the observed high and low albedo wind streaks are consistently present across multiple
221 CTX images taken years apart. The continuity between CTX images indicates that either these
222 wind streaks have been constant, experiencing a dominance of northerly sand-transporting winds
223 in their formation of at least 15+ years of CTX imaging, and that there have not been wind
224 events from other directions strong enough to erase the observed wind streaks.

225 ### *4.3 Comparison to Earth*

226   Early in its history, Mars likely had a much more Earth-like atmosphere (Pollack et al.,
227 1987; Squyres and Kasting, 1994; Carr, 1999). The much higher prevalence of craters on Mars
228 with respect to Earth makes direct comparison between Earth and Mars difficult. However,
229 topographically confined dune fields do exist on Earth. Climbing dunes on Earth have been
230 studied in a range of locations (e.g., Hack, 1941; Howard, 1985; Lancaster and Tchakerian,
231 1996), and are generally reported to form on underlying topographic slopes of <20° (White and

232 Tsoar, 1998). A wide range of factors control the dynamics of climbing dunes, including grain
233 size, wind speed, and the incidence angle with respect to topography (Tsoar, 1983; Liu et al.,
234 1999). Figure 8 illustrates a slope-limited climbing dune on Earth. Here, climbing dunes are
235 observed along the Yarlung River migrating up a slope of ~16°. About half way up the
236 mountainside the slope significantly increases to ~33°, where no dunes are observed on these
237 steeper slopes. This example demonstrates the interactions between topography and transport
238 interpreted to also be limiting the escape of aeolian material from craters on Mars. A terrestrial
239 slope limit of ~16° observed in figure 8 along with previous work done on climbing dunes on
240 Earth (Hack, 1941; Howard, 1985; Lancaster and Tchakerian, 1996, White and Tsoar, 1998) is
241 largely consistent with the slope limits observed on Mars in this work and elsewhere that
242 bedforms have difficulty migrating up slopes greater than ~15° (Chojnacki et al., 2010; Evans,
243 2012). Differences in this slope limit between Earth and Mars are small with respect to the
244 precision with which large scale topography can be measured, but any differences must be
245 attributed to the differing boundary conditions between the two planets (atmospheric density,
246 gravitational acceleration, presence of water). In both cases, sand-transport is clearly confined by
247 topography, but the bright wind streaks in this work suggest dust may not be held to the same
248 constraints on Mars.
249
250 **5 Conclusion**

251   The most prevalent basins and potential depo-centers of aeolian transported sediment on
252 Mars are craters. As a result of sediment being transported into these basins, craters can act as
253 both sources and sinks of aeolian sediment in the modern martian sedimentary cycle. Intra-crater
254 terminal dune fields and wind streaks are abundant in Arabia Terra, each indicating active
255 sediment transport and providing a way to study how wind and sediment interact with craters.
256 From the 116 craters we studied in Arabia Terra with terminal dune fields, our results show that
257 craters with low albedo wind streaks (indicative of active transport out of a crater) have lower
258 crater wall slopes (9.4° ± 5.5°) compared to craters without wind streaks (17° ± 5.8°). These two
259 end members represent basins acting as sources and sinks of sediment, respectively.

260   To better understand when sediment transport out of a crater becomes possible, we
261 focused on eight craters in the region of slope overlap between 10° - 18° that had dunes
262 migrating up slope and did not have an associated wind streak. These craters exhibited an
263 average wall slope of 14°. Previous work has identified climbing dunes on Mars migrating on
264 slopes up to 15°. The results here show that the slope of a crater wall plays a dominant role in
265 sediment transport out of a crater basin. We interpret that a crater transitions from being a net
266 sediment sink to a net sediment source when wall slopes are ~15°. This level of degradation
267 implies formation in the Noachian, suggesting post-Noachian craters on Mars trap sediment and
268 remove it from the global sediment budget.
269

References

Achilles CN, Downs RT, Ming DW, Rampe EB, Morris RV, Treiman AH, Morrison SM, Blake DF, Vaniman DT, Ewing RC, Chipera SJ., 2017, Mineralogy of an active eolian sediment from the Namib dune, Gale crater, Mars. Journal of Geophysical Research: Planets, v. 122, p. 2344–2361, doi:10.1002/2017JE005262.

Balme, M., Berman, D.C., Bourke, M.C., and Zimbelman, J.R., 2008, Geomorphology Transverse Aeolian Ridges (TARs) on Mars: v. 101, p. 703–720, doi:10.1016/j.geomorph.2008.03.011.

Banham SG, Gupta S, Rubin DM, Watkins JA, Sumner DY, Edgett KS, Grotzinger JP, Lewis KW, Edgar LA, Stack-Morgan KM, Barnes R., 2018, Ancient Martian aeolian processes and palaeomorphology reconstructed from the Stimson formation on the lower slope of Aeolis Mons, Gale crater, Mars. Sedimentology, p. 993–1042, doi:10.1111/sed.12469.

Bridges NT, Calef FJ, Hallet B, Herkenhoff KE, Lanza NL, Le Mouélic S, Newman CE, Blaney DL, De Pablo MA, Kocurek GA, Langevin Y., 2014, The rock abrasion record at Gale crater: Mars Science Laboratory results from Bradbury landing to Rocknest. Journal of Geophysical Research: Planets 119.6 1374-1389.

Bridges NT, Sullivan R, Newman CE, Navarro S, Van Beek J, Ewing RC, Ayoub F, Silvestro S, Gasnault O, Le Mouélic S, Lapotre MG.,2017, Martian aeolian activity at the Bagnold Dunes, Gale Crater: The view from the surface and orbit. Journal of Geophysical Research: Planets, v. 122, p. 2077–2110, doi:10.1002/2017JE005263.

Cabrol, N.A., and Grin, E.A., 1999, Distribution, Classification, and Ages of Martian Impact Crater Lakes: Icarus, v. 142, p. 160–172, doi:10.1006/icar.1999.6191.

Carr, M.H., 1999, Retention of an atmosphere on early Mars: Journal of Geophysical Research: Planets, v. 104, p. 21897–21909, doi:10.1029/1999JE001048.

Catling, D.C., 1999, A chemical model for evaporites on early Mars: Possible sedimentary tracers of the early climate and implications for exploration: Journal of Geophysical Research: Planets, v. 104, p. 16453–16469, doi:10.1029/1998JE001020.

Chojnacki, M., Burr, D.M., Moersch, J.E., and Michaels, T.I., 2011, Orbital observations of contemporary dune activity in Endeavor crater, Meridiani Planum, Mars: Journal of Geophysical Research: Planets, v. 116, p. 1–20, doi:10.1029/2010JE003675.

Chojnacki, M., Johnson, J.R., Moersch, J.E., Fenton, L.K., Michaels, T.I., and Bell, J.F., 2015, Persistent aeolian activity at Endeavour crater, Meridiani Planum, Mars; new observations from orbit and the surface: Icarus, v. 251, p. 275–290, doi:10.1016/j.icarus.2014.04.044.

Chojnacki, M., Moersch, J.E., and Burr, D.M., 2010, Climbing and falling dunes in valles marineris, mars: Geophysical Research Letters, v. 37, p. 1–7, doi:10.1029/2009GL042263.

Chojnacki, M., Urso, A., Fenton, L.K., and Michaels, T.I., 2017, Aeolian dune sediment flux heterogeneity in Meridiani Planum, Mars: Aeolian Research, v. 26, p. 73–88, doi:10.1016/j.aeolia.2016.07.004.

310 Craddock, R.A., Maxwell, T.A., and Howard, A.D., 1997, Crater morphometry and modification
311   in the Sinus Sabaeus and Margaritifer Sinus regions of Mars: Journal of Geophysical
312   Research: Planets, v. 102, p. 13321–13340, doi:10.1029/97JE01084.

313 Courrech du Pont, Sylvain, Clément Narteau, and Xin Gao. "Two modes for dune
314   orientation." Geology 42.9 (2014): 743-746.

315 Day, M., Edgett, K.S., and Stumbaugh, D., 2019, Ancient Stratigraphy Preserving a Wet-to-Dry,
316   Fluvio-Lacustrine to Aeolian Transition Near Barth Crater, Arabia Terra, Mars: Journal
317   of Geophysical Research: Planets, v. 124, p. 3402–3421, doi:10.1029/2019JE006226.

318 Dickson, J.L., Kerber, L.A., Fassett, C.I., and Ehlmann, B.L., 2018, A global, blended CTX
319   mosaic of mars with vectorized seam mapping: new mosaicking pipeline using principles
320   of non-destructive image editing: Lunar and Planetary Science 49, v. 10, p. 2480.

321 Edgett, K.S., 2002, Low-albedo surfaces and eolian sediment: Mars Orbiter Camera views of
322   western Arabia Terra craters and wind streaks: Journal of Geophysical Research, v. 107,
323   p. 5038, doi:10.1029/2001JE001587.

324 Edgett, K.S., and Lancaster, N., 1993, Volcaniclastic aeolian dunes: Terrestrial examples and
325   application to martian sands: Journal of Arid Environments, v. 25, p. 271–297,
326   doi:10.1006/jare.1993.1061.

327 Evan, J.R., 2012, Falling and Climbing Sand Dunes in the Cronese (" Cat ") Mountain Area , San
328   Bernardino County , California: The Journal of Geology , Vol . 70 , No . 1 (Jan ., 1962),
329   pp . 107-113 Published by : v. 70, p. 107–113.

330 Ewing, R.C., and Kocurek, G., 2010, Geomorphology Aeolian dune field pattern boundary
331   conditions: Geomorphology, v. 114, p. 175–187, doi:10.1016/j.geomorph.2009.06.015.

332 Fenton, L.K., 2006, Dune migration and slip face advancement in the Rabe Crater dune field,
333   Mars: Geophysical Research Letters, v. 33, p. 1–5, doi:10.1029/2006GL027133.

334 Grant, J.A., and Schultz, P.H., 1993, Degradation of selected terrestrial and Martian impact
335   craters: Journal of Geophysical Research, v. 98, p. 11,42, doi:10.1029/93JE00121.

336 Greeley R, Whelley PL, Arvidson RE, Cabrol NA, Foley DJ, Franklin BJ, Geissler PG,
337   Golombek MP, Kuzmin RO, Landis GA, Lemmon MT., 2006 Active dust devils in
338   Gusev crater, Mars: observations from the Mars exploration rover spirit. Journal of
339   Geophysical Research: Planets, 111, p. 1–16, doi:10.1029/2006JE002743.

340 Grotzinger JP, Bell III JF, Calvin W, Clark BC, Fike DA, Golombek M, Greeley R, Herkenhoff
341   KE, Jolliff B, Knoll AH, Malin M. W. A, Watters, 2005, Stratigraphy and sedimentology
342   of a dry to wet eolian depositional system, Burns formation, Meridiani Planum, Mars:
343   Earth and Planetary Science Letters, v. 240, p. 11–72, doi:10.1016/j.epsl.2005.09.039.

344 Grotzinger, J. P., & Milliken, R. E., 2012, The sedimentary rock record of Mars: Distribution,
345   origins, and global stratigraphy: Sedimentary Geology of Mars, 102, 1-48.

346 Hack, J. T., 1941, Dunes of the western Navajo country. Geographical Review, 31(2), 240-263.

347 Hayward, R.K., Fenton, L.K., and Titus, T.N., 2014, Mars Global Digital Dune Database
348   (MGD3): Global dune distribution and wind pattern observations: Icarus, v. 230, p. 38–
349   46, doi:10.1016/j.icarus.2013.04.011.

350 Hesse, R., 2009, Using remote sensing to quantify aeolian transport and estimate the age of the
351   terminal dune field Dunas Pampa Blanca in southern Peru: Quaternary Research, v. 71, p.
352   426–436, doi:10.1016/j.yqres.2009.02.002.

353 Howard, A.D., 1985. Interaction of sand transport with topography and local winds in the
354   northern Peruvian coastal desert. In: O.E. Barndorff-Nielsen, J.T. Mceller, K.R.
355   Rasmussen and B.B. Willetts (Editors), Proceedings of International Workshop on the
356   Physics of Blown Sand. University of Aarhus, Aarhus, pp. 511-544.

357 Fryberger, Steven G., Thomas S. Ahlbrandt, and Sarah Andrews. "Origin, sedimentary features,
358   and significance of low-angle eolian" sand sheet" deposits, Great Sand Dunes National
359   Monument and vicinity, Colorado." Journal of Sedimentary Research 49.3 (1979): 733-
360   746.

361 Kocurek, G., & Ewing, R. C., 2005, Aeolian dune field self-organization–implications for the
362   formation of simple versus complex dune-field patterns. Geomorphology, 72(1-4), 94-
363   105.

364 Kreslavsky, M.A., and Head, J.W., 2018, Mars Climate History: Insights From Impact Crater
365   Wall Slope Statistics: Geophysical Research Letters, v. 45, p. 1751–1758,
366   doi:10.1002/2017GL075663.

367 Kreslavsky, M.A., and Head, J.W., 2006, Modification of impact craters in the northern plains of
368   Mars: Implications for Amazonian climate history: Meteoritics and Planetary Science, v.
369   41, p. 1633–1646, doi:10.1111/j.1945-5100.2006.tb00441.x.

370 Lancaster, N., and V. P. Tchakerian. "Geomorphology and sediments of sand ramps in the
371   Mojave Desert." Geomorphology 17.1-3 (1996): 151-165.

372 Lee, S.W., 1984, Mars: Wind streak production as related to obstacle type and size: Icarus, v. 58,
373   p. 339–357, doi:10.1016/0019-1035(84)90080-0.

374 Liu, X., Sen, L., and Jianyou, S., 1999, Wind tunnel simulation experiment of mountain dunes:
375   Journal of Arid Environments, v. 42, p. 49–59, doi:10.1006/jare.1998.0488.

376 Mangold, N., Adeli, S., Conway, S., Ansan, V., & Langlais, B., 2012, A chronology of early
377   Mars climatic evolution from impact crater degradation. Journal of Geophysical
378   Research: Planets, 117(E4).

379 Malin MC, Bell JF, Cantor BA, Caplinger MA, Calvin WM, Clancy RT, Edgett KS, Edwards L,
380   Haberle RM, James PB, Lee SW, 2007, Context Camera Investigation on board the Mars
381   Reconnaissance Orbiter: Journal of Geophysical Research E: Planets, v. 112, p. 1–25,
382   doi:10.1029/2006JE002808.

383 Malin, M.C., and Edgett, K.S., 2000, Sedimentary Early Rocks: v. 290, p. 1927–1937.

384 McEwen AS, Eliason EM, Bergstrom JW, Bridges NT, Hansen CJ, Delamere WA, Grant JA,
385   Gulick VC, Herkenhoff KE, Keszthelyi L, Kirk RL, 2007, Mars reconnaissance orbiter's
386   High Resolution Imaging Science Experiment (HiRISE): Journal of Geophysical
387   Research: Planets, v. 112, p. 1–40, doi:10.1029/2005JE002605.

388 McKee, E. D. (1979). A study of global sand seas. US Govt. Print. Off.

McLennan SM, Bell Iii JF, Calvin WM, Christensen PR, Clark BD, De Souza PA, Farmer J, Farrand WH, Fike DA, Gellert R, Ghosh A, 2005, Provenance and diagenesis of the evaporite-bearing Burns formation, Meridiani Planum, Mars: Earth and Planetary Science Letters, v. 240, p. 95–121, doi:10.1016/j.epsl.2005.09.041.

McLennan, S.M., Grotzinger, J.P., Hurowitz, J.A., and Tosca, N.J., 2019, The Sedimentary Cycle on Early Mars: Annual Review of Earth and Planetary Sciences, v. 47, p. 91–118, doi:10.1146/annurev-earth-053018-060332.

Montgomery, D.R., Bandfield, J.L., and Becker, S.K., 2012, Periodic bedrock ridges on Mars: Journal of Geophysical Research E: Planets, v. 117, p. 1–12, doi:10.1029/2011JE003970.

Newsom, H. E., Brittelle, G. E., Hibbitts, C. A., Crossey, L. J., & Kudo, A. M., 1996, Impact crater lakes on Mars. Journal of Geophysical Research: Planets, 101(E6), 14951-14955.

Pollack, J.B., Kasting, J.F., Richardson, S.M., and Poliakoff, K., 1987, The case for a wet, warm climate on early Mars: Icarus, v. 71, p. 203–224, doi:10.1016/0019-1035(87)90147-3.

Robbins, S.J., and Hynek, B.M., 2012, A new global database of Mars impact craters ≥1 km: 1. Database creation, properties, and parameters: Journal of Geophysical Research: Planets, v. 117, p. 1–18, doi:10.1029/2011JE003966.

Robbins, S.J., Hynek, B.M., Lillis, R.J., and Bottke, W.F., 2013, Large impact crater histories of Mars: The effect of different model crater age techniques: Icarus, v. 225, p. 173–184, doi:10.1016/j.icarus.2013.03.019.

Sharp, R. P, 1966,. Kelso Dunes, Mojave Desert, California. Geological Society of America Bulletin, 77(10), 1045-1074.

Rubin, D. M., & Hunter, R. E.,1987, Bedform alignment in directionally varying flows. Science, 237(4812), 276-278.

Silvestro, S., Fenton, L.K., Vaz, D.A., Bridges, N.T., and Ori, G.G., 2010, Ripple migration and dune activity on Mars: Evidence for dynamic wind processes: Geophysical Research Letters, v. 37, p. 5–10, doi:10.1029/2010GL044743.

Smith DE, Zuber MT, Frey HV, Garvin JB, Head JW, Muhleman DO, Pettengill GH, Phillips RJ, Solomon SC, Zwally HJ, Banerdt WB., 2001, Mars Orbiter Laser Altimeter: Experiment summary after the first year of global mapping of Mars: Journal of Geophysical Research E: Planets, v. 106, p. 23689–23722, doi:10.1029/2000JE001364.

Squyres, S.W., and Kasting, J.F., 1994, Early mars: How warm and how wet? Science, v. 265, p. 744–749, doi:10.1126/science.265.5173.744.

Stopar, J.D., Robinson, M.S., Barnouin, O.S., McEwen, A.S., Speyerer, E.J., Henriksen, M.R., and Sutton, S.S., 2017, Relative depths of simple craters and the nature of the lunar regolith: Icarus, v. 298, p. 34–48, doi:10.1016/j.icarus.2017.05.022.

Thomas, P., Veverka, J., Lee, S., and Bloom, A., 1981, Classification of wind streaks on Mars: Icarus, v. 45, p. 124–153, doi:10.1016/0019-1035(81)90010-5.

Tsoar, Haim. "Wind tunnel modeling of echo and climbing dunes." Developments in Sedimentology. Vol. 38. Elsevier, 1983. 247-259.

428 Urso, Anna, Matthew Chojnacki, and David A. Vaz. "Dune-Yardang Interactions in Becquerel
429   Crater, Mars." Journal of Geophysical Research: Planets 123.2 (2018): 353-368.

430 Veverka, J., Gierasch, P., and Thomas, P., 1981, Wind streaks on Mars: Meteorological control
431   of occurence and mode of formation: Icarus, v. 45, p. 154–166, doi:10.1016/0019-
432   1035(81)90011-7.

433 Ward, A.W., 1979, Yardangs on Mars: Evidence of recent wind erosion: Journal of Geophysical
434   Research, v. 84, p. 8147, doi:10.1029/jb084ib14p08147.

435 White, B.R., and Tsoar, H., 1998, Slope effect on saltation over a climbing sand dune:
436   Geomorphology, v. 22, p. 159–180, doi:10.1016/S0169-555X(97)00058-5.

437 Wordsworth, R.D., 2016, The Climate of Early Mars: Annual Review of Earth and Planetary
438   Sciences, v. 44, p. 381–408, doi:10.1146/annurev-earth-060115-012355.

439 Zimbelman, James R., and Lora J. Griffin. "HiRISE images of yardangs and sinuous ridges in
440   the lower member of the Medusae Fossae Formation, Mars." Icarus 205.1 (2010): 198-
441   210.

442
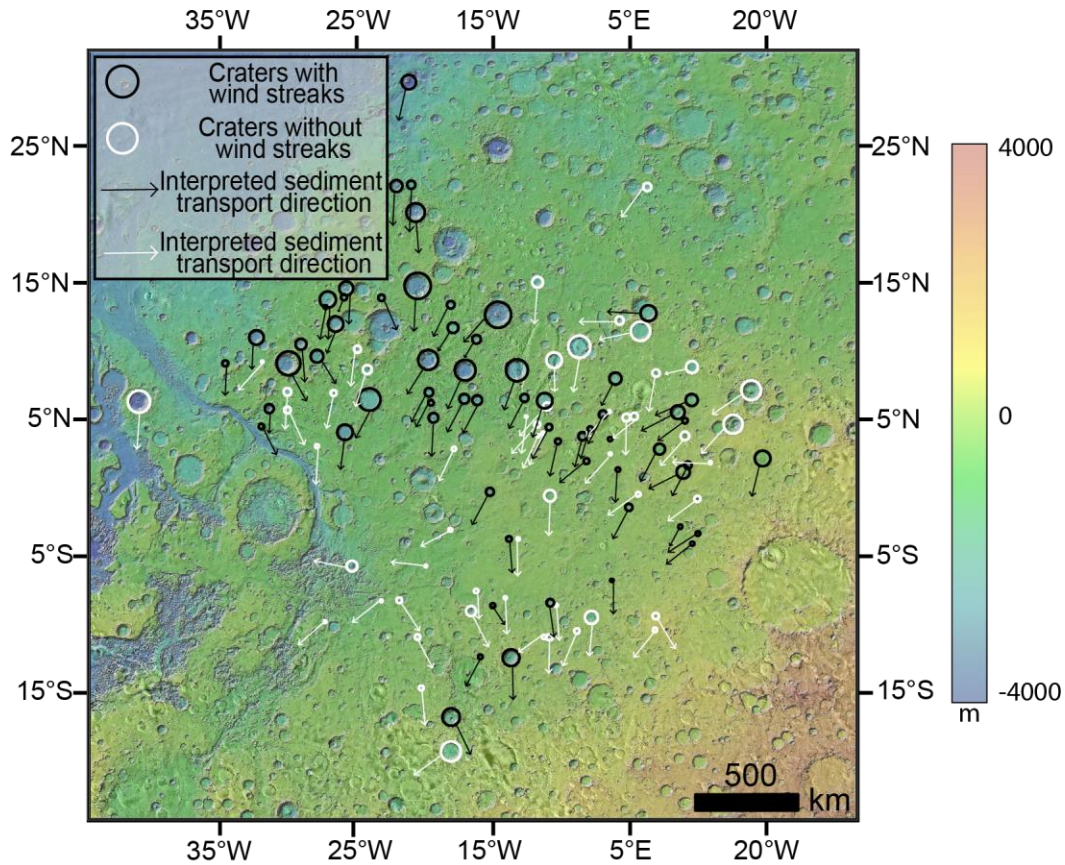
Figure 1. *Craters with terminal dune fields and their interpreted wind directions in Arabia Terra, Mars.* Black circles show studied crater basins exhibiting wind streaks. White circles show studied craters without wind streaks. The black and white arrows associated with the craters show the interpreted prevailing wind directions based on dune morphology, position of terminal dune field within the craters, and wind streak orientation. Colorized MOLA elevation over CTX mosaic basemap.

449
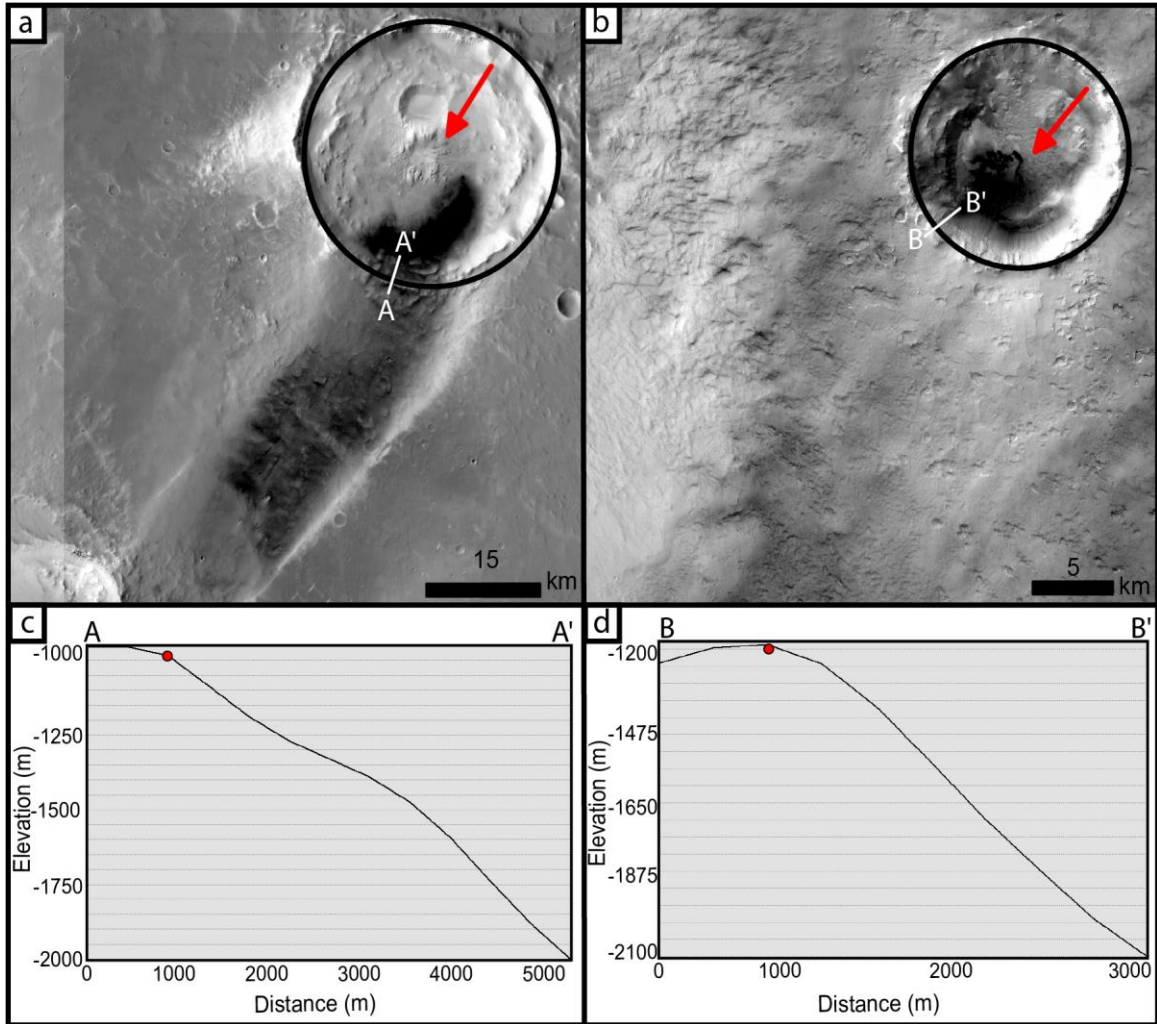
Figure 2. *Crater basins with terminal dune fields.* **(a)** A terminal dune field (dark region in crater interior) abutted against a crater wall, with a slope of ~15°, served as a sediment source for the downwind wind streak. Centered on 2.83° E, 9.75° N. **(b)** A crater with a trapped terminal dune field (dark region in crater interior) against a crater wall with a slope of ~21°. Unlike (a), no discernible material is being transported out of this crater. Crater rims are outlined in black and red arrows indicate the downwind direction of sand-transporting winds. Centered on 356.74° E, 0.78° N. **(C)** and **(D)** show the elevation profiles of each crater. Red dot indicates the crater rim location. CTX mosaic basemap.

458

459
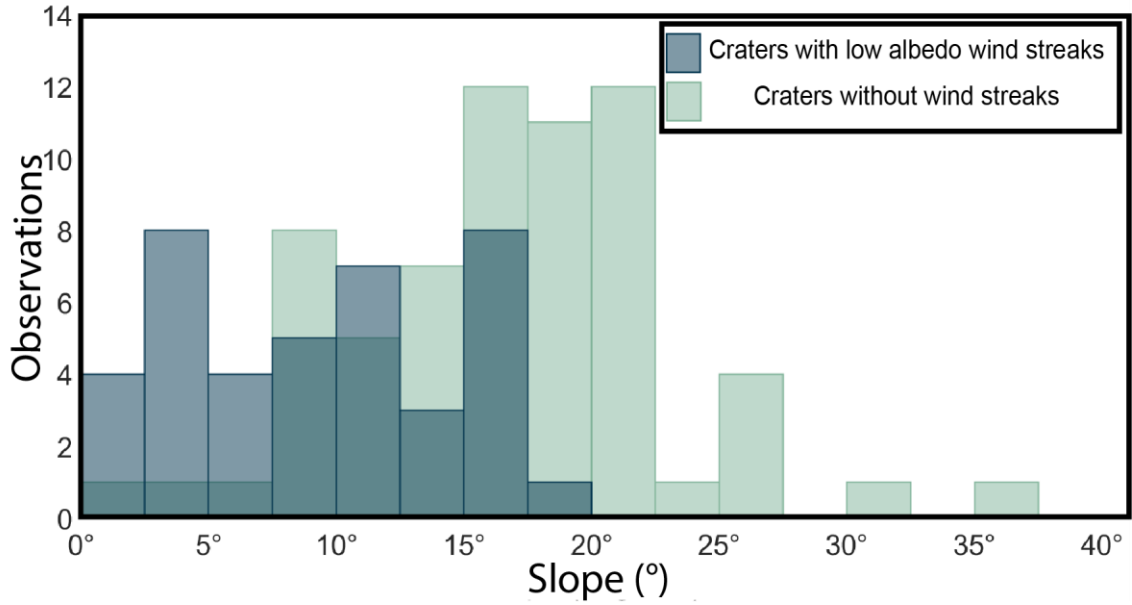
Figure 3. *Histogram of crater wall slopes measured in craters with and without wind streaks.*
Craters with low albedo wind streaks, and therefore interpreted to exhibit transport of sediment
out of the crater, display lower slopes when compared to craters without wind streaks which
exhibit more steeply inclined crater walls. The slope range where a crater transistions from being
a sink to a source is between 10° and 20°.
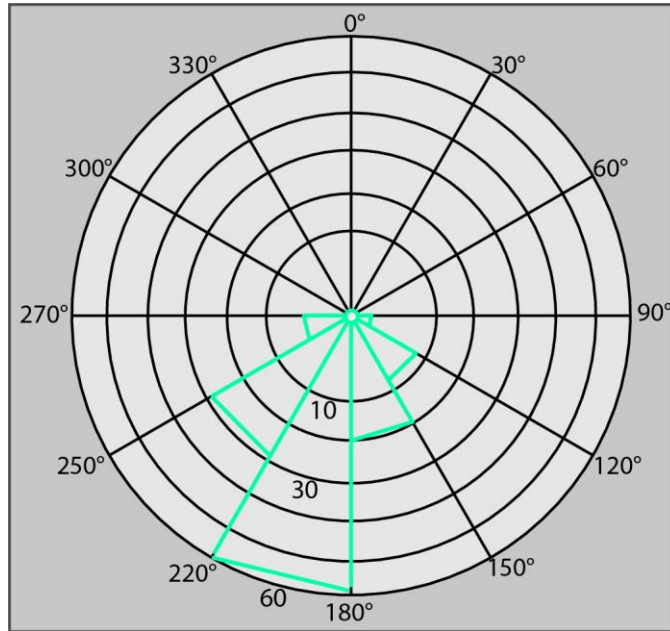
465
Figure 4. *Rose diagram of interpreted wind directions of all 116 craters identified in this study.*
Wind direction is dominantly towards the south

468
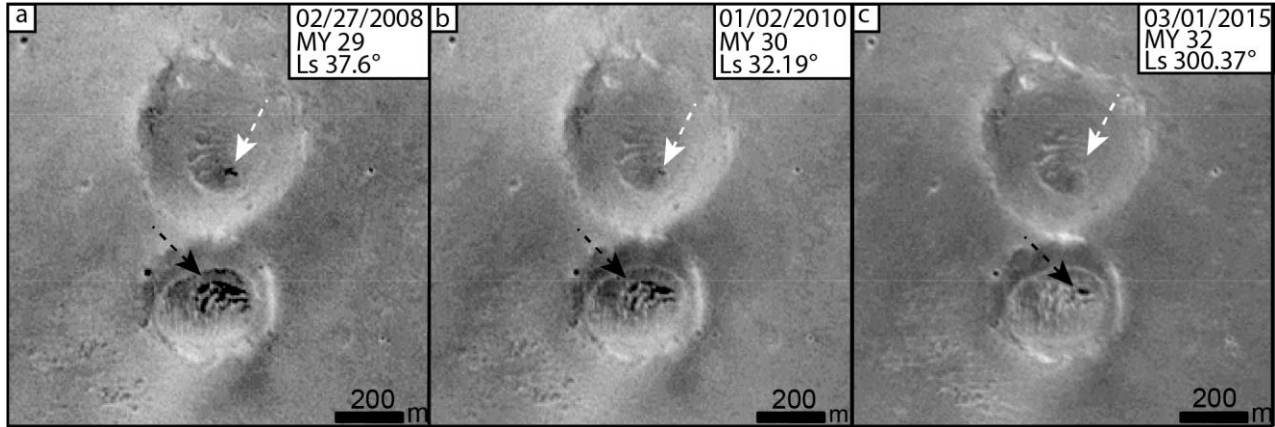
469

470 **Figure 5**. *Dune fields observed in two craters within a low albedo wind streak over a 3 martian*
471 *year timespan.* Black and white arrows indicate the location of each dune field in their respective
472 craters. Images a – c show a decrease in the volume of sediment comprising the dunes over time
473 in each crater indicating that active sediment transport is occurring within the low albedo wind
474 streak. Craters are within a wind streak emanating from crater #15 (see supplement) North is up
475 in all images. CTX image IDs: (a) F12_040287_1896_XI_09N357W, (b)
476 B17_016103_1889_XN_08N357W, (c) P16_007440_1867_XI_06N357W.
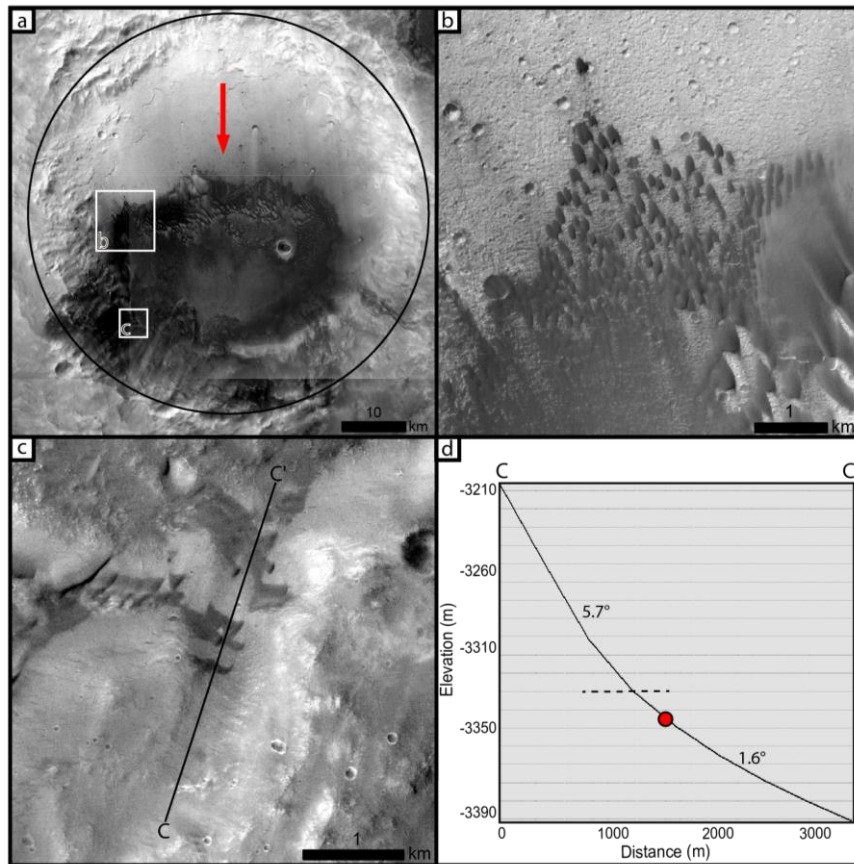
477

478 **Figure 6**. *Dune fields migrating up a crater wall (crater #60 in supplement).* **a)** There is no wind
479 streak out of the crater. Dune field is migrating towards the south shown by the red arrow. White
480 boxes show locations of (b) and (c). **b)** Dunes migrating across the crater floor towards the crater
481 wall. **c)** Image showing slope measurement of first slope encountered by dunes moving across

482 the crater floor. There are no dunes seen past ~6 km up the crater's wall. d) elevation profile of
483 slope measurement in (c). North is up in all images. CTX image
484 P19_008614_1892_XI_09N016W
485
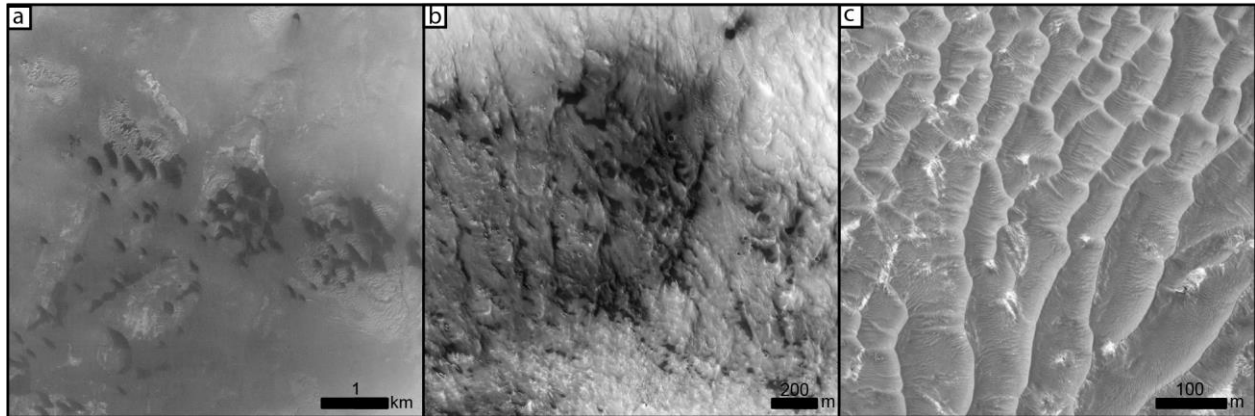
486
487 **Figure 7**. *Aeolian features observed within low albedo wind streaks.* **a)** Dune fields are present
488 within several low albedo wind streaks, however, only when low albedo wind streaks extend into
489 another crater. Dunes in 'a' are located within crater #113 (see supplement). **b)** Low albedo
490 features without a well-defined crestline are common throughout each low albedo wind streak.
491 These features are primarily seen abutted against a topographic feature that impedes their
492 migration and promotes accumulation of sediment. **c)** TAR like bedforms are the most common
493 feature found within a low albedo wind streak. Wavelengths between their crests measure
494 between 50 – 70 m. A direction of transport is difficult to discern in each instance due to the
495 symmetry of the feature. North is up in all images. CTX image ID: (a)
496 P11_005462_1836_XI_03N351W; HiRISE images (b) ESP_019439_1975; (c)
497 ESP_047157_1850
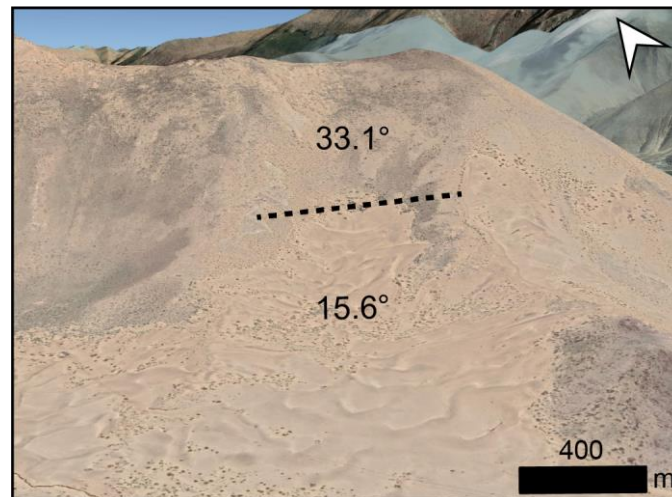
498
499 **Figure 8**. *Climbing dunes on Earth.* Foreground bedforms migrate up a mountain slope found
500 along the Yarlung River, China, but dunes do not reach the peak of the mountain. Dashed line
501 indicates a change in slope, above which dunes are not observed. Perspective view centered on
502 29.28°N, 91.79°E with white arrow indicating north. Image courtesy of Google Earth. Measured
503 slope value indicated on the image obtained from the Advanced Spaceborne Thermal Emission
504 and Reflection Radiometer (ASTER) dataset.
505

506

Wind streak type	Crater wall slope	Number of craters
Low albedo	9.4° ±5.5°	39
High albedo	24.4° ±9.6°	16
No wind streak	17.0° ±5.8°	61
		Total: **116**

507

508 **Table 1.** *Summary of crater wall slopes measured in observed crater basins.*

509

Wind streak type	Diameter range (km)	Average diameter ± 1 σ (km)	depth/diameter ratio (*μ* ± 1 σ)
Low albedo	16 – 111	49 ± 23	0.03 ± 0.01
High albedo	13 – 111	46 ± 31	0.04 ± 0.01
No wind streak	10 - 95	32 ± 22	0.05 ± 0.02

510 **Table 2.** *Summary of crater diameters and d/D within each wind streak type.*

511